

Sensitivity of Idealized Hurricane Intensity and Structures under Varying Background Flows and Initial Vortex Intensities to Different Vertical Resolutions in HWRF

DA-LIN ZHANG AND LIN ZHU

Department of Atmospheric and Oceanic Science and Center for Scientific Computation and Mathematical Modeling, University of Maryland, College Park, College Park, Maryland

XUEJIN ZHANG

Cooperative Institute for Marine and Atmospheric Studies, University of Miami, and NOAA/Atlantic Oceanographic and Meteorological Laboratory, Miami, Florida

VIJAY TALLAPRAGADA

NOAA/NCEP/Environmental Modeling Center, College Park, Maryland

(Manuscript received 1 April 2014, in final form 8 November 2014)

ABSTRACT

A series of 5-day numerical simulations of idealized hurricane vortices under the influence of different background flows is performed by varying vertical grid resolution (VGR) in different portions of the atmosphere with the operational version of the Hurricane Weather Research and Forecasting Model in order to study the sensitivity of hurricane intensity forecasts to different distributions of VGR. Increasing VGR from 21 to 43 levels produces stronger hurricanes, whereas increasing it further to 64 levels does not intensify the storms further, but intensity fluctuations are much reduced. Moreover, increasing the lower-level VGRs generates stronger storms, but the opposite is true for increased upper-level VGRs. On average, adding mean flow increases intensity fluctuations and variability (between the strongest and weakest hurricanes), whereas adding vertical wind shear (VWS) delays hurricane intensification and then causes more rapid growth in intensity variability. The stronger the VWS, the larger intensity variability and bifurcation rate occur at later stages. These intensity differences are found to be closely related to inner-core structural changes, and they are attributable to how much latent heat could be released in higher-VGR layers, followed by how much moisture content in nearby layers is converged. Hurricane intensity with higher VGRs is shown to be much less sensitive to varying background flows, and stronger hurricane vortices at the model initial time are less sensitive to the vertical distribution of VGR; the opposite is true for relatively uniform VGRs or weaker hurricane vortices. Results reveal that higher VGRs with a near-parabolic or Ω shape tend to produce smoother intensity variations and more typical inner-core structures.

1. Introduction

High-resolution cloud-resolving modeling of hurricanes has become practically commonplace in recent years, even at some operational centers [e.g., NOAA/National Centers for Environmental Prediction (NCEP)]. Increasing horizontal resolution of hurricane models has indeed shown promising results in the reproduction of storm sizes

and inner-core structures, including eyewall convection, spiral rainbands, and eyewall replacements (Yau et al. 2004; Chen et al. 2011). Despite the significant structural improvements, some studies show relatively small variations in hurricane intensity forecasts when the finest nested grid lengths are varied between 5 and 1 km (Fierro et al. 2009; Davis et al. 2010). Zhang et al. (2011) and Gopalakrishnan et al. (2011) showed statistically similar results using the Hurricane Weather Research and Forecasting (HWRF) Model as the finest grid length decreases from 9 to 3 km. The above results indicate that simply decreasing the grid length of cloud-resolving models to a few kilometers does not always lead to

Corresponding author address: Dr. Da-Lin Zhang, Department of Atmospheric and Oceanic Science, University of Maryland, College Park, 2419 CSS Bldg., College Park, MD 20742-2425.
E-mail: dalin@atmos.umd.edu

better prediction of hurricane intensity. This result may be attributed partly to the dependence of some physics parameterizations on horizontal resolution, and partly to the inconsistency between the horizontal and vertical grid resolution (VGR; Lindzen and Fox-Rabinovitz 1989). Of particular relevance is that Zhang and Wang (2003, hereafter ZW), and Kimball and Dougherty (2006, hereafter KD) have shown substantial differences in the simulated hurricane intensity when VGRs are varied.

Specifically, ZW showed that a nested-grid version of the fifth-generation Pennsylvania State University–National Center for Atmospheric Research Mesoscale Model (MM5) with the finest horizontal grid length of 6 km and the model top of 50 hPa could produce significant impact on the intensity and inner-core cloud/precipitation structures of Hurricane Andrew (1992), a category 5 storm, in their 72-h sensitivity simulations by varying VGR between 23 and 69 layers. For the VGRs tested, the minimum surface central pressure could range from 932 to 899 hPa (dropped from its initial value of 1010 hPa), the azimuthally averaged peak tangential winds from 60 to 90 m s⁻¹, inflows in the planetary boundary layer (PBL) from 30 to 40 m s⁻¹, updrafts from 2.5 to 4.5 m s⁻¹, and diabatic heating rates from 50 to 80 K h⁻¹. Later, KD examined the sensitivity of the model-simulated hurricane intensity, size, and inner-core structures to the vertical distribution of VGR, also using the MM5 model but with the model top of 100 hPa and variable surface layer thicknesses (between 39 and 348 m), an idealized hurricane-like vortex in the absence of background flow, and the finest grid length of 5 km. By varying the vertical distribution of VGR at 24 levels, as compared to 35 levels, KD found a much greater intensity range (i.e., between 899 and 964 hPa at the strongest stage) in their 8.5-day simulations than that seen by ZW. This different intensity variability might be partly attributed to the fact that Hurricane Andrew reaches landfall near 72 h into the integration.

Of significance is that changing VGR in different atmospheric layers could produce different hurricane intensities and inner-core structures. For example, ZW showed that increasing the low-level VGR is more efficient in intensifying a hurricane, whereas changing the upper-level VGR has little impact on the hurricane intensity. They found that the increased hurricane intensity is related to the increased latent heat release in the lower troposphere, which is consistent with the previous findings that the low-level heating maximum is more efficient than the upper-level one in spinning up mesoscale cyclones (Tracton 1973; Anthes and Keyser 1979; Zhang and Fritsch 1988). In addition, both ZW and KD showed that the use of a thicker surface layer

tends to produce higher maximum surface winds and more surface heat fluxes, leading to the development of a stronger storm.

In contrast, KD reached a somewhat different conclusion from that of ZW. That is, increasing upper-level VGRs tends to produce a stronger storm whereas “a well-resolved inflow layer does not necessarily correspond to an intense storm.” They speculated that the generation of such a stronger storm results from increased mass fluxes in the upper-level outflow layer. However, it is unclear how increasing the upper-level VGR could increase the upper outflow mass flux because it may be a result of intensifying storms. The different conclusions could not be explained by the different MM5 configurations and initial conditions they used, but just allude to our limited knowledge on the roles of VGR in determining hurricane intensity.

Thus, the major objectives of this study are to examine (i) to what extent the above two different conclusions are valid, (ii) how varying VGRs can affect hurricane intensity forecasts under different background flows consisting of both mean and vertical wind shear (VWS), and (iii) how sensitive VGRs are to different rotational speeds at the model initial time. The objectives will be achieved by studying systematically the sensitivity of hurricane intensity simulations to VGRs using the operational version of the HWRF Model (Gopalakrishnan et al. 2011; Bao et al. 2012; Tallapragada et al. 2013) with the finest grid length of 3 km, and idealized hurricane-like vortices under different background flows. As compared to real-data cases (e.g., in ZW), the advantages of using idealized initial conditions include the absence of vertical interpolation errors, and of inhomogeneous external forcing parameters, such as sea surface temperature (SST), and background flows. This work will also reveal how the HWRF Model is sensitive to the vertical distribution of VGR and help design a more optimal distribution of VGR for the operational hurricane model.

The next section describes the basic features of the HWRF Model. Section 3 presents experimental designs for all the sensitivity simulations to be conducted. Section 4 examines the sensitivity of the model-simulated hurricane intensity to the varying VGRs and background flows as well as different initial vortex intensities. Section 5 shows diagnostic analyses of the structural differences in order to help gain insight into why certain VGR configurations tend to produce stronger storms than the others.

2. Model description

In this study, the model grid setup and physics options are configured as closely as possible to the current

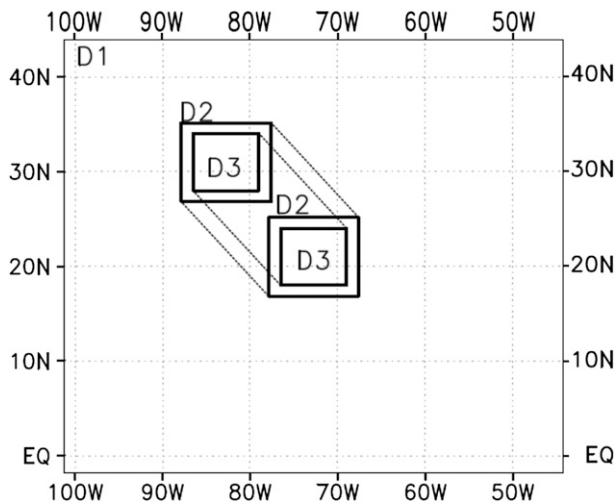


FIG. 1. The nested-grid domains with the grid length of 27 km in D1, 9 km in D2, and 3 km in D3. Domains D2 and D3 move northwestward from the central region of domain D1. Latitudes and longitudes are provided to indicate the domains' sizes and the Earth's rotational effect.

operational HWRF system (Gopalakrishnan et al. 2011; Yeh et al. 2012; Bao et al. 2012; Tallapragada et al. 2013), which uses the same dynamical core as NCEP's WRF-Nonhydrostatic Mesoscale Model (NMM; Janjić et al. 2001, Janjić 2003). The major features of the HWRF Model used include the following: (i) a two-way interactive, movable, triply-nested (27/9/3 km) grid procedure (Fig. 1), but with 50% of the tendencies of all prognostic variables fed back from finer- to coarser-mesh domains; (ii) the simultaneous use of the simplified Arakawa–Schubert scheme (Han and Pan 2006) and the Ferrier (1994, 2005) cloud microphysics scheme for the 27- and 9-km resolution domains, but only the latter for the 3-km resolution domain; (iii) the Eta Geophysical Fluid Dynamics Laboratory (GFDL) longwave and shortwave radiation schemes (Schwarzkopf and Fels 1991; Lacis and Hansen 1974); and (iv) the GFDL surface layer (Kwon et al. 2010) and PBL (Hong and Pan 1996; Gopalakrishnan et al. 2013) schemes. To minimize the computational time, the Ferrier cloud microphysics scheme is executed every 3 min, close to that used in the 2012 operational HWRF version.

The three nested-grid domains D1, D2, and D3 have (x, y) areas of $8559 \text{ km} \times 8343 \text{ km}$, $1566 \text{ km} \times 1521 \text{ km}$, and $1131 \text{ km} \times 903 \text{ km}$, with 27-, 9-, and 3-km grid length, respectively. Note that shorter lengths are used in the north–south directions because of the easterly mean flow used for the idealized simulations (Fig. 1). Finer-mesh domains are allowed to move freely within coarser domains such that the storm center can always be maintained in the middle portion of the finer-mesh domains.

The HWRF Model is initialized, following Gopalakrishnan et al. (2011), by an axisymmetric hurricane-like vortex embedded in an easterly mean flow with a specified vertical wind shear (VWS). All the model runs are terminated at 120 h, at which time most of the simulated storms reach a steady state except under the influence of strong VWS. The environmental temperature and humidity fields are based on Jordan's Caribbean sounding (Gray et al. 1975). A constant SST of 302 K is assumed as the bottom forcing over all the three domains.

Figures 2a and 2b show the vertical distribution of $\delta\sigma$ (i.e., σ -layer thickness) and σ levels, respectively. Here, the terrain-following coordinate σ is defined as

$$\sigma = \frac{p - p_t}{p_s - p_t}, \quad (1)$$

where p is the pressure, p_s is the surface pressure, and $p_t = 50 \text{ hPa}$ is the pressure at the model top, unless otherwise stated. The vertical coordinate of the HWRF Model follows closely the hybrid σ – p coordinate system used in the WRF-NMM dynamic core (Janjić 2003; Janjić et al. 2010; Arakawa and Lamb 1977) where the upper levels of the atmosphere above 420 hPa (σ top) are defined by hydrostatic pressure levels, while the levels below 420 hPa are described by the terrain-following σ coordinates. To define the different σ levels and the shape of $\delta\sigma$ curves, the corresponding σ values at the pressure levels above 420 hPa are calculated using the following equation:

$$p = \sigma_1 \times \text{PD}_{\text{top}} + \sigma_2 \times \text{PD} + p_t, \quad (2)$$

where PD_{top} is the difference between the model top pressure (p_t) and pressure at the interface of σ – p coordinates; and PD is the difference between surface pressure and pressure at the interface of σ – p coordinates (Janjić et al. 2010). Both σ_1 and σ_2 are constants defined for vertical level assignments. For the pressure coordinates above 420 hPa, σ_2 is set to zero.

In HWRF, $\delta\sigma$ is defined by a functional form with a near-parabolic shape (Eckermann 2009), with higher VGRs in the lower and upper portions, and coarser VGRs in the middle portion of the atmosphere (Fig. 2). Such a near-parabolic shape in $\delta\sigma$ has also been used in the early cloud modeling studies of Liu et al. (1997) and Zhu et al. (2004) with 23 σ levels, albeit not as smooth as that shown in Fig. 2a. For the current operational model, in which 43 σ levels are used (referred to as OPN43), $\delta\sigma$ varies from 0.00492 for the top layer to 0.0080301 for the layer immediately above the surface layer, and the coarsest VGR of 0.04228 appears in the midtroposphere (i.e., near $\sigma = 0.5$). The difference in thickness between the coarsest and highest resolution σ layers for OPN43 is more than 8 times.

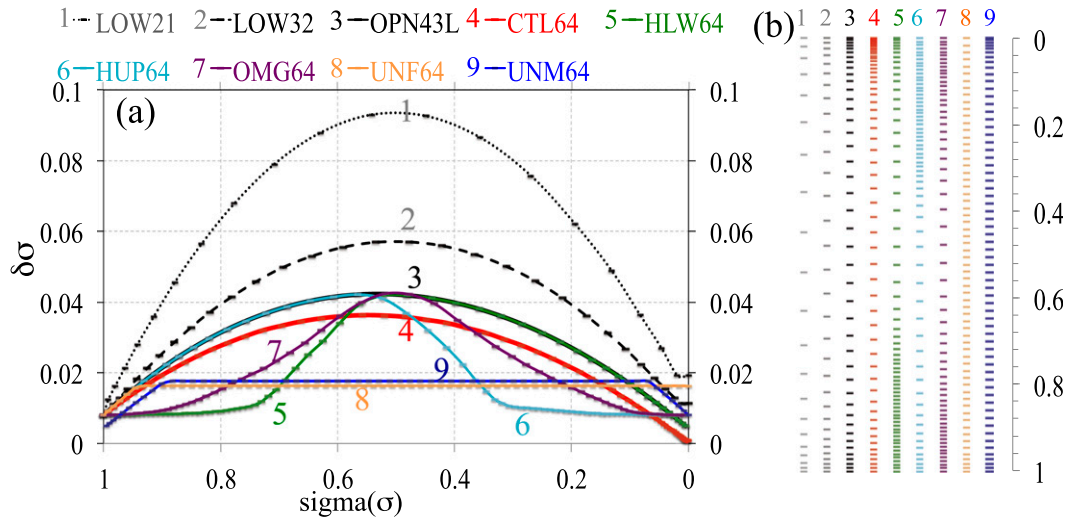


FIG. 2. (a) Distribution of the VGR ($\delta\sigma$) as a function of σ , and (b) vertical distribution of σ levels, for the 43-level operational prediction (3: OPN43, thick black), the 64-level control (4: CTL64, thick red), the lower-VGR 32 levels (2: LOW32, black dashed), the lowest-VGR 21 levels (1: LOW21, black dotted), 64 levels with higher VGRs at the low levels (5: HLW64, green), 64 levels with higher VGRs at the upper levels (6: HUP64, light blue), the 64-level Ω shape (7: OMG64, purple), 64 levels with a uniform VGR above $\sigma = 0.9$ (8: UNF64, orange), and 64 levels with a uniform VGR in the layer $\sigma = 0.9-0.1$ (9: UNM64, dark blue). The same colors are used for individual time series shown in Figs. 3–9 and 13.

3. Experimental design

To achieve the objectives of this study, two classes or nine types of sensitivity experiments need to be carried out to test the influences of different VGRs on hurricane intensity (see Fig. 2). Class 1 deals with different VGRs but keeps the same near-parabolic shape of $\delta\sigma$ distribution as that in OPN43; that is, by (i) increasing proportionally the number of vertical levels from 43 levels in OPN43 to 64 levels (CTL64), or by decreasing it proportionally to (ii) 32 (LOW32), and (iii) 21 (LOW21) levels, respectively. For class 2, the following five types of sensitivity experiments are performed, using both CTL64 and OPN43 as the control experiments (i.e., increasing the number of vertical levels from 43 to 64 in various ways), to examine the effects of changing the vertical distribution of VGR: increase the VGR in (i) the lower (i.e., $\sigma = 0.7-1.0$) layers (HLW64); (ii) the top (i.e., $\sigma = 0-0.3$) layers (HUP64); (iii) increase the number of vertical levels to 64 with a high and uniform VGR in the layers above $\sigma = 0.9$ (UNF64); (iv) as in (iii), but for the $\sigma = 0.9-0.1$ layers (UNM64: a high uniform VGR in the middle portion of the atmosphere), while keeping the other portions of VGR identical to OPN43; and (v) increase the VGRs in OPN43 in both the lower and upper troposphere, but decrease it in the midtroposphere [i.e., making an Ω shape (OMG64)]. Table 1 lists all the nine types of numerical experiments, including the two different types of control experiments.

Note that in the above experiment design, only half of HLW64 and HUP64 is different from that of OPN43, so half of the OPN43 curve is identical to the HLW64 curve, while the other half is identical to the HUP64 curve (Fig. 2a). The Ω shape so designed has similar VGRs in the lowest (top) 100 hPa to those associated with HLW64 (HUP64), and similar VGRs in the middle layers to those associated with OPN43. Note also that the surface layer thickness in all the simulations remains identical, namely, keeping $\delta\sigma = 0.0080301$ (roughly 18 m). This setting is necessary because the surface layer thickness affects the magnitude of the simulated surface winds, which in turn influences surface heat flux calculations and hurricane intensity (see ZW and KD).

Since hurricane intensity could also be determined by the magnitudes of mean flow and VWS, among the other environmental conditions, the above-mentioned experiments will be performed using the same axisymmetric hurricane-like vortex [with an initial maximum surface wind (V_{MAX}) of 20 m s^{-1} , VMAX20] but under the influence of the following six different easterly background flows: (i) no mean flow and no VWS (V0S0); (ii) a -5 m s^{-1} mean flow but no VWS (V5S0); (iii) a -2.5 m s^{-1} VWS (defined between 100 and 1000 hPa) with no mean flow (V0S2.5); (iv) a -5 m s^{-1} VWS with no mean flow (V0S5); (v) a -2.5 m s^{-1} VWS with a -5 m s^{-1} mean flow (V5S2.5); and (vi) a -5 m s^{-1} VWS with a -5 m s^{-1} mean flow (V5S5).

Another set of sensitivity simulations is conducted in the same way as the above experiments (vi) except for

TABLE 1. Two classes of sensitivity experiments and their associated intensity variability [ΔP_{MIN} (hPa) and ΔV_{MAX} (m s^{-1})] under varying background flows (V and VWS) at the end of the 5-day integrations.

Index	Expt	Remarks	ΔP_{MIN} (hPa)	ΔV_{MAX} (m s^{-1})
1	LOW21	Decrease the number of vertical levels from 43 to 21	35	21
2	LOW32	Decrease the number of vertical levels from 43 to 32	35	22
3	OPN43	43 vertical levels as the current operational HWRF Model	34	19
4	CTL64	Increase the number of vertical levels from 43 to 64	26	9
5	HLW64	Increase the VGR for the layers in $\sigma = 0.7\text{--}1.0$, while keeping the rest the same as in OPN43, with a total of 64 levels	28	6
6	HUP64	Increase the VGR for the layers in $\sigma = 0\text{--}0.3$, while keeping the rest the same as in OPN43, with a total of 64 levels	44	27
7	OMG64	Increase the number of vertical levels to 64 from OPN43, but with a Ω shape (i.e., higher VGRs at the lower and upper levels, but coarser VGRs in the midtroposphere)	33	16
8	UNF64	Increase the number of vertical levels to 64, with a uniform and higher VGRs for the layers above $\sigma = 0.9$	47	20
9	UNM64	Increase the number of vertical levels to 64, with a uniform and higher VGRs for the layers in $\sigma = 0.9\text{--}0.1$, while keeping the other layers the same as OPN43	48	27

using a stronger initial vortex (i.e., $V_{\text{MAX}} = 35 \text{ m s}^{-1}$) in order to examine the sensitivity of hurricane intensity forecasts to VGRs due to different rotational speeds at the model initial time (VMAX35). The background flow of V5S5 is used only for VMAX35 because of the generation of greater intensity variability than the other flow conditions, as will be shown in the next section. Thus, a total of 63 five-day numerical simulations, plus a few additional experiments to test the impact of the model top level, are performed to examine the sensitivity of the simulated hurricane intensity to VGRs, while leaving all the other model configurations untouched.

4. Results

In this section, the sensitivity of varying VGR is examined mainly in terms of hurricane intensity [i.e., the minimum sea level pressure (P_{MIN}) and the maximum surface wind (V_{MAX})]. More focus will also be placed on the magnitude of (i) intensity variability, defined as the difference between the strongest and weakest storms, (ii) extreme (i.e., more rapid or slower) deepeners, and (iii) the trend in intensity changes as the VGR and background flow are varied. Because the time series of P_{MIN} is smoother than that of V_{MAX} , the former will be more often used herein to indicate the intensity variability of different sensitivity simulations. The variations of the simulated hurricane tracks due to different VGRs are not discussed, because they are small (not shown), as also shown by ZW in the sensitivity study of Hurricane Andrew (1992). Our results are presented below in accordance with the four different combinations of mean flow and VWS plus one different V_{MAX} at the initial time.

a. The absence of mean flow and VWS

Figure 3 shows the time series of P_{MIN} and V_{MAX} from all the nine VGR runs in the absence of mean flow and VWS (V0S0). We see that all the hurricane vortices intensify in similar fashion with little variability in intensity changes during the first 24 h of the simulations, in which the mass and wind fields are adjusting toward each other while spinning up about 20 hPa in P_{MIN} . Subsequently, intensity changes among the nine VGR runs begin to diverge rapidly until 36–42 h into the integrations, after which period the diverging intensity range remains nearly constant, albeit with intersections of some time series. On average, the simulated hurricane vortices intensify about 60 hPa or $20\text{--}30 \text{ m s}^{-1}$ with an intensity variability of $\Delta P_{\text{MIN}} = 29 \text{ hPa}$ and $\Delta V_{\text{MAX}} = 22 \text{ m s}^{-1}$ near the end of the 120-h integrations (Table 2). These results show clearly the sensitivity of HWRF to different VGRs. Note that the intensity variability (and the mean storm deepening rate) so obtained is about 75% of (or 5–10 hPa weaker than) the ZW-simulated category 5 storms, but it is only 55% of (or about 50 hPa weaker than) the idealized storms of KD.

An analysis of the model sensitivity simulations in class 1 reveals that LOW21 always produces the weakest storm during the 120-h simulation, whereas LOW32 tends to produce the strongest one, although it shows slightly weaker intensities than those produced by OPN43 and CTL64 at some hours (Fig. 3). This result implies that increasing the VGR from 21 to 32 levels tends to intensify hurricane vortices, which is consistent with the conclusions of ZW and KD; but increasing it further to 43 and 64 levels does not generally result in stronger storms, which is clearly opposite to the results of ZW and KD. As will be shown in section 5, the latter could be attributed to the

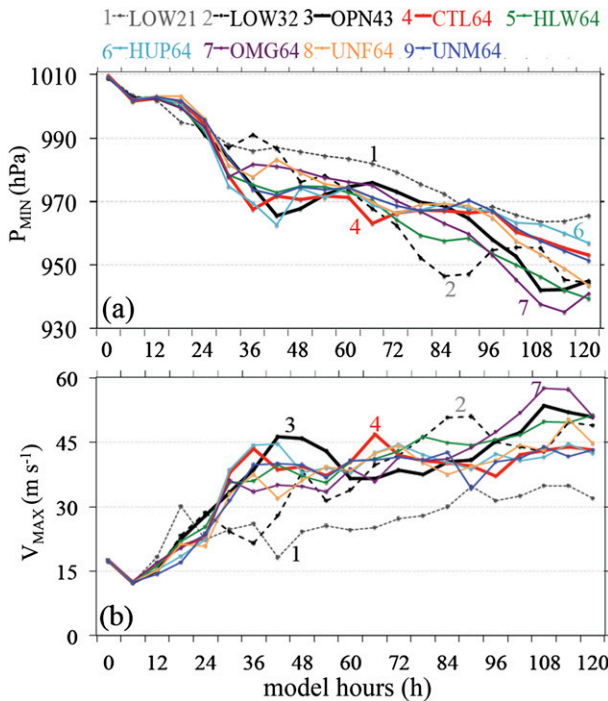


FIG. 3. Comparisons of the 120-h model-simulated (a) minimum central pressure (hPa) and (b) maximum surface wind speed (m s^{-1}) at 3-hourly intervals from the VGRs associated with the 43-level operational prediction (3: OPN43, thick black), the 64-level control (4: CTL64, thick red), the lower-VGR 32 levels (2: LOW32, black dashed), the lowest-VGR 21 levels (1: LOW21, black dotted), 64 levels with higher VGRs at the low levels (5: HLW64, green), 64 levels with higher VGRs at the upper levels (6: HUP64, light blue), the 64-level Ω shape (7: OMG64, purple), 64 levels with an uniform VGR above $\sigma = 0.9$ (8: UNF64, orange), and 64 levels with an uniform VGR in the layer $\sigma = 0.9\text{--}0.1$ (9: UNM64, dark blue) under the influence of no mean flow and no VWS (i.e., V0S0). An initial vortex intensity of $V_{\text{MAX}} = 20 \text{ m s}^{-1}$ is used. See Fig. 2 for the index, acronym, and contour color conventions used.

generation of different storm structures as the VGR increases to a certain extent. Nevertheless, the results imply that there might be an optimal distribution of VGRs for hurricane models. Note that while the CTL64 (LOW32) storm is generally weaker (stronger) among the class-1 simulations, it exhibits smaller (larger) intensity fluctuations after the 36-h simulations.

It is also apparent from Fig. 3 that OMG64 in class 2 tends to produce a storm that is close to the mean intensity of all the simulated storms during the 2–4-day simulations, but the strongest one subsequently. As compared to the corresponding control run (i.e., CTL64), increasing the lower and upper layer VGRs produces a weaker (stronger) storm during the 2–3 (3–5) day simulation with the peak differences of 10 hPa in P_{MIN} and 12 m s^{-1} in V_{MAX} . Increasing the VGR in the lower half of the troposphere (HLW64), while keeping it identical to that in OPN43 in the layers above, produces a storm that is on average 2–5 hPa stronger than that in both OPN43 and CTL64 after the 2.5-day simulation, but it is similar in intensity to that in OMG64. This result indicates the significance of increasing the lower-level VGR in deepening the model hurricane, which conforms to the work of ZW.

In contrast, increasing the VGRs in the upper-half portion of the model atmosphere (HUP64), while keeping it identical to that in OPN43 in the layers below, produces a storm that is similar in intensity to that in both OPN43 and CTL64 during the first 3.5-day simulation, but a 2–10-hPa weaker storm subsequently. The same is also true for the upper-level outflow strength, as will be shown in section 5. This result contradicts that of KD, in which a much stronger storm develops as the upper-level VGRs increase, as mentioned in section 1.

Increasing the VGRs from OPN43 in the middle portion of the atmosphere (i.e., between the PBL and $\sigma = 0.12$, UNM64) produces a storm that resembles CTL64 in intensity after the 3-day integration. Similarly, increasing the VGRs from OPN43 in the layers above the PBL (i.e., UNF64) generates a storm that is between CTL64 and OPN43 in intensity. A more notable difference between UNF64 and UNM64 is the VGR in the layers above $\sigma = 0.12$ (see Fig. 2), indicating again that increasing the upper-level VGRs tends to produce a weaker storm. The impact on the simulated storm intensity due to the small difference in $\delta\sigma$ in the layers between the PBL and $\sigma = 0.12$ appears to be negligible.

It is apparent from the above analyses that there is little evidence to suggest the generation of a stronger storm by increasing the upper-level VGRs. Since experimental

TABLE 2. The magnitudes of intensity variability [ΔP_{MIN} (hPa) and ΔV_{MAX} (m s^{-1})], the strongest and weakest storms in terms of P_{MIN} , and the model hour (at which ΔP_{MIN} between the strongest and weakest storms is peaked), under varying background flows (V and VWS).

Index	Background flow	ΔP_{MIN} (hPa)	ΔV_{MAX} (m s^{-1})	Strongest (hPa)	Weakest (hPa)	Model hour (h)
i	V0S0	29	22	OMG64 (935)	LOW21 (964)	114
ii	V5S0	23	35	HLW64 (959)	LOW21 (982)	120
iii	V0S2.5	39	37	OPN43 (947)	LOW21 (986)	114
iv	V0S5	47	35	OMG64 (953)	HUP64 (1000)	120
v	V5S2.5	28	24	HLW64 (970)	UNM64 (998)	96
vi	V5S5	37	26	HLW64 (964)	HUP64 (1001)	114

setups between **KD** and the present study are similar, except for the different model tops used, we have conducted three additional sensitivity simulations with the model top set at 100 hPa and 43 levels in the vertical: (i) a reference run with the same $\delta\sigma$ shape as CTL43 (CTL_TOP); (ii) a sensitivity run with higher VGR in the upper half of the model atmosphere (HUP_TOP), that is, having a $\delta\sigma$ shape similar to HUP64; and (iii) a sensitivity run with a uniform VGR above $\sigma = 0.8$ (UNF_TOP), that is, having a $\delta\sigma$ shape similar to UNF64. Note that UNF_TOP has VGRs that are coarser than HUP_TOP and CTL_TOP above $\sigma = 0.3$ and $\sigma = 0.2$, respectively.

Results indicate that HUP_TOP produces the weakest storm, then CTL_TOP and UNF_TOP after the 2-day integration, with the peak differences of 15 hPa in P_{MIN} and 8 m s^{-1} in V_{MAX} among the three runs at the end of the 5-day integration (not shown). Clearly, these results confirm those of **ZW** and are consistent with those of HUP64. Thus, we may state that the different intensity results from those of **KD**, on the impact of the upper-level VGR, may be attributed to the other aspects of model configurations, such as the MM5 dynamics core, cloud microphysics parameterization, air–sea interaction treatment, variable surface layer thicknesses, and too coarse VGR (e.g., 24 levels). Although exploring it thoroughly is beyond the scope of the present study, some simulations presented below exhibit higher sensitivities and fluctuations of storm intensity when coarser VGRs or too high VGRs at the upper levels are used (Table 1).

b. Influence of a mean flow

Since a moving hurricane may experience different structural and intensity changes from a stationary one on accessing “fresh” air in the PBL ahead (Frank and Ritchie 1999; Peng et al. 1999), it is desirable to examine how sensitive hurricane intensity changes are to the VGRs under the influence of varying background flows. Figure 4 shows that on average the simulated hurricane vortices under the influence of a 5 m s^{-1} easterly flow (V5S0) intensify about 40 hPa and 20 m s^{-1} with the intensity variability of $\Delta P_{\text{MIN}} = 23 \text{ hPa}$ and $\Delta V_{\text{MAX}} = 35 \text{ m s}^{-1}$ (or $\Delta P_{\text{MIN}} = 15 \text{ hPa}$ and $\Delta V_{\text{MAX}} = 15 \text{ m s}^{-1}$ if excluding the outlier of LOW21). Although these quantitative changes are much smaller than those associated with the V0S0 storms, fluctuations in V_{MAX} are more pronounced, especially for the simulations with coarser VGRs. These results indicate clearly the dependence of the VGR sensitivity on the mean flow, among several other environmental properties (e.g., moisture content). Moreover, a comparison of the OPN43 storm with that of V0S0 indicates the weakening of hurricanes after adding a mean flow, which was also found by Peng et al. (1999). They attributed this weakening to the asymmetry

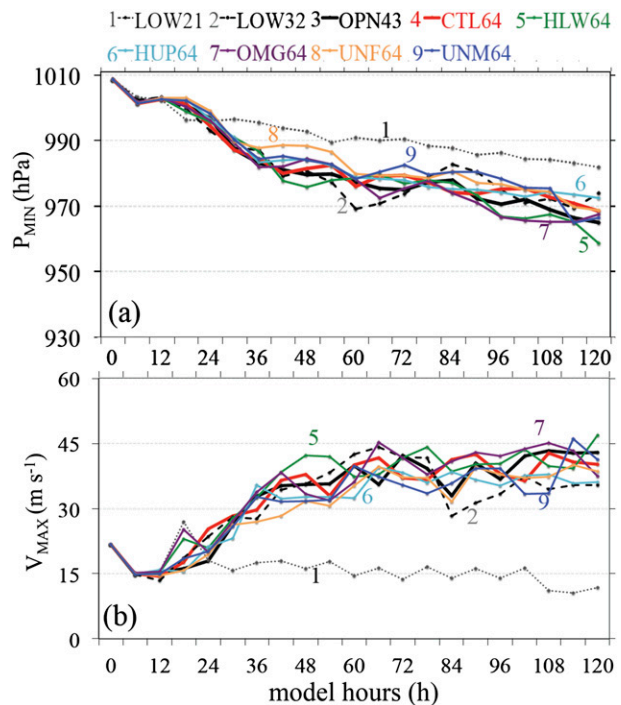


FIG. 4. As in Fig. 3, but for the influence of a 5 m s^{-1} easterly flow (i.e., V5S0).

induced by surface friction and the phase difference between moisture convergence and surface flux. In the present case, this weakening is related to the drier PBL air in the immediate environment, seen in height–radius cross sections, that converges into the storm (not shown).

Results obtained from the class-1 simulations with V5S0 are generally similar to those with V0S0. That is, increasing VGR from 21 to 32 and 43 levels tends to intensify the storms, but increasing it further to 64 levels generates a weaker storm. Again, the LOW21 storm appears to be the weakest one among all the simulations (Fig. 4), even with slight weakening trends in V_{MAX} during the 5-day integrations; it is indeed an outlier. This result suggests that *some minimum VGR is required for hurricane models in order to produce more reliable intensity forecasts*. The minimum required VGR appears to occur between 21 and 32 levels for the HWRF configurations used herein, especially for the given horizontal resolution. This conclusion could be further seen from the simulations that follow next, but with different background flow conditions.

Adding a mean flow to V0S0 also shows more frequent appearances of stronger storms at various hours as higher VGRs are placed in the lower troposphere (i.e., HLW64 and OMG64). By comparison, increasing VGRs in the upper troposphere (i.e., HUP64) shows more frequent appearances of weaker storms than those in OPN43 and CTL64 as well as HLW64, ending up with a weak

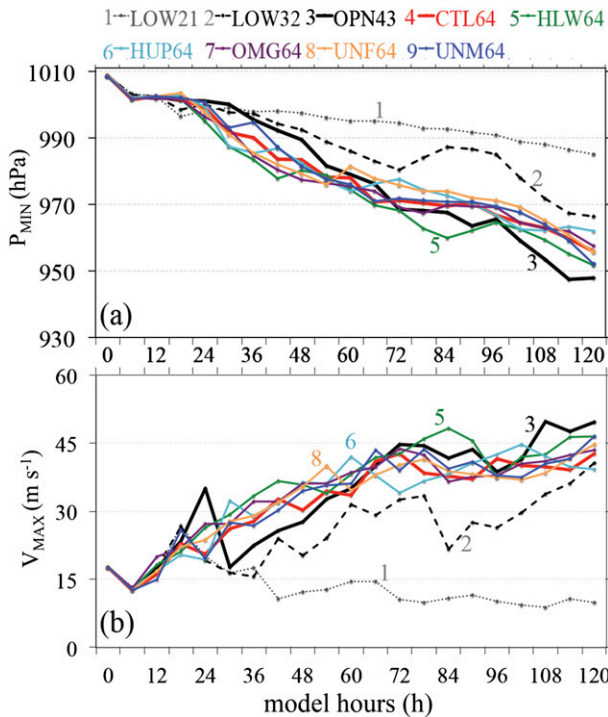


FIG. 5. As in Fig. 3, but for the influence of a 2.5 m s^{-1} easterly VWS (i.e., VOS2.5).

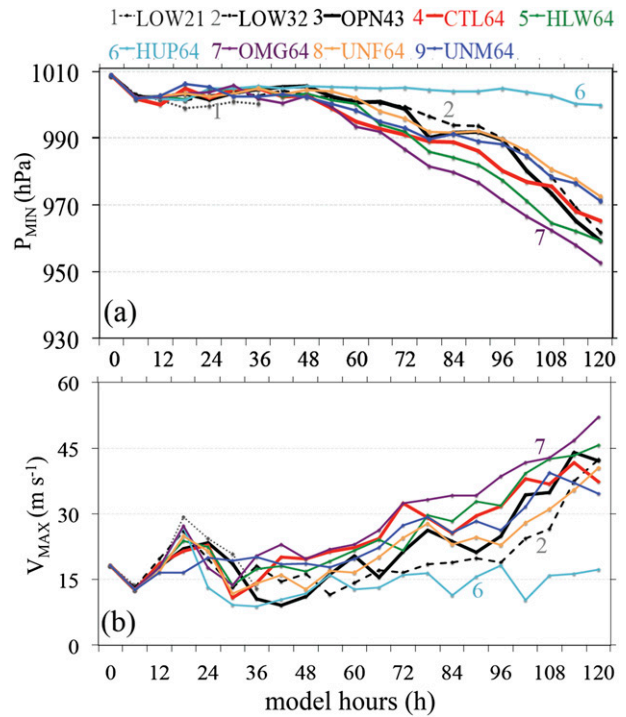


FIG. 6. As in Fig. 3, but for the influence of a 5 m s^{-1} easterly VWS (i.e., VOS5).

intensity next to LOW21. The peak intensity differences between HUP64 and HLW64 are about 15 hPa in P_{MIN} and 10 m s^{-1} in V_{MAX} (Figs. 4a,b). On the other hand, increasing the midlevel VGRs (e.g., UNF64 and UNM64) produces relatively weaker storms than those in CTL64 and OPN43. Tests of the other mean flows are not shown because similar conclusions could be qualitatively reached.

c. Influence of vertical wind shear

It is well known that VWS could exert an important impact on the structures, intensity, and predictability of hurricanes (Wang and Holland 1996; Frank and Ritchie 1999, 2001; Zhu et al. 2004; Zhang and Tao 2013). In general, adding VWS to VOS0 tends to delay the deepening of P_{MIN} , and to produce weaker storms at the end of the 5-day integrations (cf. Figs. 5 and 3). The stronger VWS that are imposed, the weaker the storms that are produced (cf. Figs. 5 and 6). These results are qualitatively consistent with the previous observational and modeling studies (Frank and Ritchie 1999, 2001; Black et al. 2002). Of interest are the generation of larger intensity variability under the influence of stronger VWS (i.e., VOS2.5 vs VOS5) at the end of the 5-day integration (see Table 2), and the different temporal intensity variations from the simulations without mean flow or VWS. For example, the strongest storm under VOS2.5 is produced by OPN43 with $P_{\text{MIN}} = 947 \text{ hPa}$ and $V_{\text{MAX}} = 50 \text{ m s}^{-1}$,

whereas the weakest storm is produced by LOW21 with $P_{\text{MIN}} = 986 \text{ hPa}$ and $V_{\text{MAX}} = 10 \text{ m s}^{-1}$ at the end of the 5-day simulations (Fig. 5), resulting in the intensity variability of $\Delta P_{\text{MIN}} = 39 \text{ hPa}$ and $\Delta V_{\text{MAX}} = 40 \text{ m s}^{-1}$. By comparison, the strongest storm under VOS5 is produced by OMG64 with $P_{\text{MIN}} = 953 \text{ hPa}$ and $V_{\text{MAX}} = 52 \text{ m s}^{-1}$, whereas the weakest storm is produced by LOW21 in $V_{\text{MAX}} (=14 \text{ m s}^{-1})$, but by HUP64 in $P_{\text{MIN}} (=1000 \text{ hPa})$, which is unexpected, at the end of the 5-day simulations (Fig. 6), resulting in the intensity variability of $\Delta P_{\text{MIN}} = 47 \text{ hPa}$ and $\Delta V_{\text{MAX}} = 48 \text{ m s}^{-1}$. It follows that greater sensitivity to VGR appears in the presence of stronger VWS. This result is consistent with the findings of Zhang and Tao (2013) that reduced predictability of hurricane intensity occurs in the presence of larger VWS. Note that the previously mentioned delays in the deepening of storms extend to 48–60 h into the integrations in the presence of stronger VWS, and more pronounced bifurcations in intensity change occur afterward within the time series envelope of the OMG64 and HUP64 (and LOW21) storms (Fig. 6). This indicates that hurricane models, at least for intensifying storms, are less (more) sensitive to VGRs in the presence of strong VWS during the first 2–3-day (3–5 day) integrations or during the slow (fast) intensifying stages.

Unlike the results shown in the preceding two subsections, we see from Fig. 6 that under the influence of

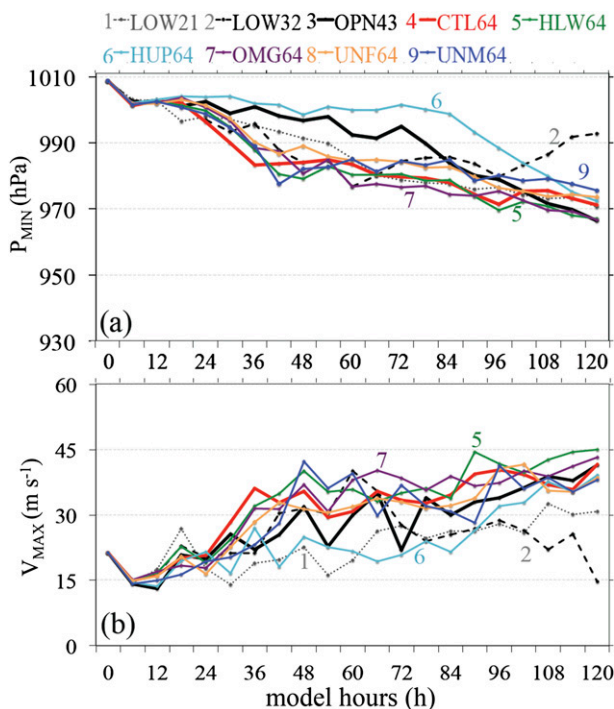


FIG. 7. As in Fig. 3, but for the influence of a 5 m s^{-1} easterly flow with a 2.5 m s^{-1} easterly VWS (i.e., V5S2.5).

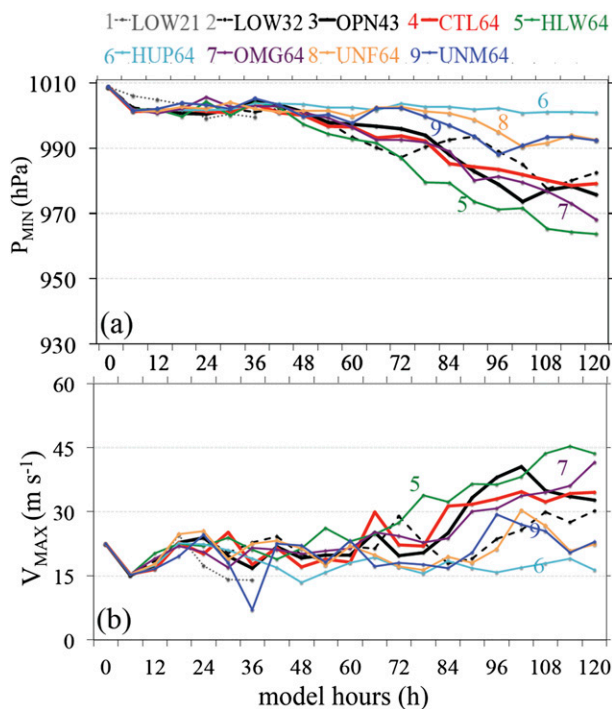


FIG. 8. As in Fig. 3, but for the influence of a 5 m s^{-1} easterly flow with a 5 m s^{-1} easterly VWS (i.e., V5S5).

stronger VWS (i.e., V0S5), (i) CTL64 produces a (5–6 hPa) stronger storm more frequently than OPN43, as can be expected from ZW's work; and (ii) LOW21 produces unexpectedly a deeper storm in P_{MIN} than OPN43 (and several other simulations) most times. In addition, while OPN43 produces a stronger storm at the end of the 5-day simulations, the HLW64 storm, next to the OMG64 storm, exhibits stronger intensities at most of the other times under both V0S2.5 and V0S5 cases (Figs. 5 and 6), confirming further the significance of increasing the lower-level VGRs in producing stronger storms. Also of note is that the OPN43 storm under the weaker VWS case (i.e., V0S2.5) displays the largest fluctuation in V_{MAX} among all the sensitivity simulations during the 18–30-h integrations (Fig. 5b). A similar fluctuation in V_{MAX} also occurs under the stronger VWS case (i.e., V0S5), albeit with a smaller amplitude (Fig. 6b).

d. Influence of mean flow and vertical wind shear combined

When a -5 m s^{-1} mean flow is superimposed with two different VWS, we see some different or nonlinear behaviors among the sensitivity simulations. That is, under the influence of V5S2.5 (Fig. 7), the strongest storm in P_{MIN} (V_{MAX}) is produced by OPN43 and HLW64, similar to that under V0S2.5, whereas the weakest storm is produced more or less by UNM64 (and LOW32), giving

rise to an intensity variability of $\Delta P_{\text{MIN}} = 33 \text{ hPa}$ and $\Delta V_{\text{MAX}} = 30 \text{ m s}^{-1}$ at the end of the 5-day simulation. In contrast, under the influence of V5S5 (Fig. 8), the strongest storm is produced by HLW64, whereas like under V0S5, the weakest storm is produced by LOW21 and HUP64, resulting in an intensity variability of $\Delta P_{\text{MIN}} = 37 \text{ hPa}$ and $\Delta V_{\text{MAX}} = 27 \text{ m s}^{-1}$ at the end of the 5-day simulation. The time series of the LOW21 storms is terminated after the 36-h simulations under both V0S5 (Fig. 6) and V5S5 (Fig. 8) because little closed circulation could be seen in the surface wind field. Of interest is that the HUP64 storm deepens after the 84-h integration under V5S2.5 (Fig. 7), even with an intensity close to that of the CTL64 storm at the end of the 120-h simulations, whereas it remains the weakest storm most of the hours under V0S5 and V5S5 (Figs. 6 and 8). As will be shown in section 5, the different results can be attributed to the development of localized updrafts in the eyewall.

Of importance is that although differences in the intensity variability between the weak and strong VWS cases—V0S2.5 vs V0S5 (cf. Figs. 5 and 6) and V5S2.5 vs V5S5 (cf. Figs. 7 and 8)—are similar in magnitude at the end of the 5-day integrations, intensity bifurcation rates are smaller in the former than in the latter cases during the later stages. This confirms the earlier finding that hurricane intensity forecasts are more sensitive to VGRs

in the presence of intense VWS. In fact, Figs. 5 and 7 show that the intensity variability under weak VWS (e.g., V0S2.5 and V5S2.5) remains nearly constant after the first 36–48-h integrations. By comparison, Figs. 6 and 8 show that the intensity variability under strong VWS (e.g., V0S5 and V5S5) will likely continue to increase if the simulations are extended beyond 5 days.

Note that the rapid intensity bifurcation rates occur with more pronounced fluctuations in V_{MAX} after the 24-h integrations under V5S2.5 (i.e., by adding a weak VWS to V5S0) (cf. Figs. 7 and 4), but such rapid bifurcation is delayed under V5S5 to 60 h into the integrations with little intensity changes prior, which is similar to that under V0S5 (cf. Figs. 8 and 6). Again, more fluctuations in V_{MAX} are associated with relatively coarser VGRs, such as LOW21, LOW32, and OPN43, after adding a weak VWS to V5S0 (cf. Figs. 7 and 4), and to a certain extent under the other background flow conditions (Figs. 3, 5, 6, and 8).

e. Sensitivity of hurricane intensity to different VGRs under varying background flows

After seeing the sensitivity of the model-simulated hurricane intensity to different VGRs under the influence of a given background flow, it is of interest to examine how sensitive each VGR configuration is to varying background flows. It is evident from Table 1 that the final intensity produced by CTL64 (HLW64) is the least sensitive in terms of P_{MIN} (V_{MAX}) to varying background flows, with the lowest value of 953 hPa (44 m s^{-1}) under V0S0 and the highest value of 979 hPa (35 m s^{-1}) under V5S5, giving an intensity variability of $\Delta P_{MIN} = 26 \text{ hPa}$ ($\Delta V_{MAX} = 9 \text{ m s}^{-1}$). In contrast, UNM64 (HUP64) is the most sensitive in terms of P_{MIN} (V_{MAX}) to varying background flows, with the lowest value of 951 hPa (44 m s^{-1}) under V0S0 and the highest value of 999 hPa (20 m s^{-1}) under V5S2.5, resulting in an intensity variability of $\Delta P_{MIN} = 48 \text{ hPa}$ ($\Delta V_{MAX} = 24 \text{ m s}^{-1}$); UNF64 ($\Delta P_{MIN} = 47 \text{ hPa}$) is ranked the next to UNM64, and then LOW32 and LOW21. Among all the simulations, OMG64 produces the strongest storm ($P_{MIN} = 935 \text{ hPa}$, $V_{MAX} = 57 \text{ m s}^{-1}$) under V0S0, whereas the weakest storm is produced by HUP64 in terms of P_{MIN} ($=1001 \text{ hPa}$) under both V0S5 and V5S5 (see Table 2). (The LOW21 storm has kept dissipating under either V0S5 or V5S5, again with little evidence of a closed surface circulation after the 36-h simulations.)

It is also of interest to see a nonlinear relationship between the intensity variability with different VGRs and the varying background flows. First, in general, LOW21 produces the slow deepening of P_{MIN} , and even pronounced spindown of V_{MAX} from its initial intensity, becoming an outlier under V5S0, V0S2.5, V0S5, and V5S5. This further suggests the importance of using

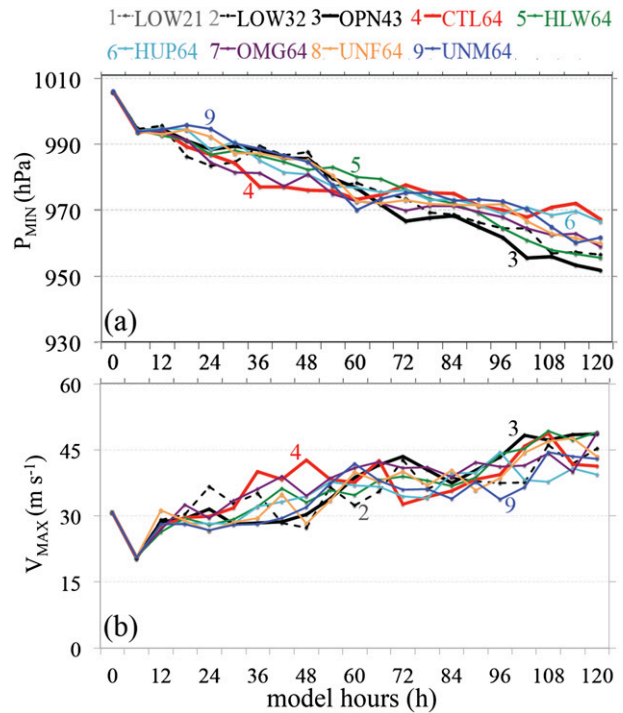


FIG. 9. As in Fig. 3, but with $V_{MAX} = 35 \text{ m s}^{-1}$ at the model initial time under the influence of a 5 m s^{-1} easterly flow with a 5 m s^{-1} easterly VWS (i.e., V5S5).

VGRs that are consistent with the horizontal resolution used; more than 21 vertical levels should be used for the HWRF Model with the 3-km grid length. Second, on average, OMG64 tends to produce a stronger storm, at least at some stages, under the influence of V0S0, V5S0, V0S5, V5S2.5, and V5S5. This result also demonstrates the significance of increasing the lower-level VGRs in generating a stronger storm. Third, while HUP64 tends to produce weaker storms, especially as compared to HLW64, its simulated storms under the influence of large VWS (i.e., either V0S5 or V5S5) exhibit little intensity changes in both P_{MIN} and V_{MAX} during the 5-day simulations; similarly for UNM64 under V5S2.5. Such a scenario also occurs under V0S2.5 during the first 84-h integrations; similarly for UNM64 under V5S5. In this regard, the storms produced by HUP64 as well as LOW21 and UNM64 appear to be outliers in character in hurricane intensity forecasts, and their use should clearly be avoided.

f. Influence of initial vortex intensity

Since the above results show the generation of greater intensity variability in the presence of stronger VWS, another nine experimental simulations with an idealized vortex of $V_{MAX} = 35 \text{ m s}^{-1}$ at the model initial time (i.e., VMAX35) are conducted under V5S5. With VMAX35, Fig. 9 shows much reduced intensity

variability of $\Delta P_{\text{MIN}} = 19 \text{ hPa}$ ($\Delta V_{\text{MAX}} = 16 \text{ m s}^{-1}$), compared to $\Delta P_{\text{MIN}} = 37 \text{ hPa}$ and $\Delta V_{\text{MAX}} = 26 \text{ m s}^{-1}$ in the case of VMAX20 (Fig. 8). Of note is that excluding the outlier of LOW21 the intensity variability of the VMAX35 storms remains nearly constant after the 24-h simulations, whereas that of the VMAX20 storms still keeps increasing at the end of the 5-day simulations. The reduced variability characteristics also occur under the other background flows (not shown). This may be intuitively understandable, because the presence of larger inertial stability associated with an initially stronger vortex tends to resist changes in VGR and likely the other settings unless the VGR is too coarse. Some other general conclusions obtained in the preceding subsections also apply to the VMAX35 storms, such as reduced storm intensity as the VGR increases from 43 to 64, and the generation of stronger (weaker) storms when the low (upper) level VGR is increased.

5. Relationship between intensity and inner-core structural variations

In this section, diagnostic analyses are performed in an attempt to gain insight into why the simulated hurricane intensities are sensitive to different VGRs under the influence of varying background flows. Since hurricanes are driven by diabatic heating, all the intensity differences are attributable to different inner-core structures and magnitudes in latent heat release within the storms. Thus, the simulated rainfall and flow fields from a few representative experiments under the influence of V0S0 and V5S5 are examined below, both from the 114-h simulations when more marked intensity differences are present.

Apparently, use of different VGRs could also produce large differences in the inner-core structures of rainfall and rotational flows as well as their intensities (Fig. 10), indicating further the importance of designing appropriate distribution of VGRs. For example, the weakest storm of LOW21 under V0S0 exhibits the smallest coverage of rainfall, most of which is limited within the radius of 100 km, with little evidence of spiral rainbands in the outer region (Fig. 10a). In contrast, the stronger storm of HLW64 has the widest coverage of rainfall, up to the radius of 200 km (Fig. 10d). Moreover, more spiral rainbands could be seen beyond the radius of 300 km, albeit less organized. This tends to block energy supply to the eyewall regions (Powell 1990). Hence, the HLW64 storm may have been stronger without rainbands in the outer regions. Of relevance is that rainfall coverage increases with more spiral rainbands as the VGR increases from 21 to 43 and then 64 (Figs. 10a–c); similarly when the lower-level VGRs are increased

from OPN43 [e.g., HLW64 (Fig. 10d) and OMG64 (not shown)]. This impact appears to be equivalent to that of increasing horizontal resolution in the study of [Yau et al. \(2004\)](#), who show much improved representation of spiral rainbands associated with Hurricane Andrew (1992) as the finest grid length is decreased from 6 to 2 km. Despite the increased rainfall coverage, hurricane intensity does not increase proportionally, due likely to the development of spiral rainbands in the outer region. As compared to HLW64, increasing the upper-level VGRs (HUP64 and UFM64) produces much smaller rainfall coverage (cf. Figs. 10e,f and 10d). However, its coverage is close to that of OPN43 since their lower-level VGRs are identical; the different intensities between HUP64 and OPN43 are again attributable to the development of outer rainbands.

An important question one may ask is the following: why does increasing the low-level VGR facilitate the intensification of hurricanes, whereas increasing the upper-level VGR produces weaker storms? Based on the area-averaged vertical profiles of latent heat release, [ZW](#) indicate that the gridbox saturation tends to take place earlier and faster when higher VGRs in the lower troposphere are used. Vertical cross sections of the azimuthally averaged secondary circulations, given in Fig. 11, provide further evidence to support [ZW](#)'s analyses. For instance, the LOW21 storm exhibits the shallowest secondary circulations with the weakest radial inflows and outflows, whereas the increased VGRs in OPN43 produces a strong storm at this time in terms of P_{MIN} , V_{MAX} , and the upper-level outflow strength (cf. Figs. 11b and 3). (Note the development of an updraft above $z = 6 \text{ km}$ in the core region, shown in Fig. 11a, which represents part of asymmetries resulting from the use of the nonconstant Coriolis parameter.) *Such a positive correlation between hurricane intensity and upper-level outflow strength is consistent with that found by KD. However, increasing the upper-level VGR does not lead to the generation of stronger upper outflows (cf. Figs. 11b,e), which is opposite to the results of KD. This could also be seen from Figs. 11d and 11e, showing that HUP64 and HLW64 produce peak outflows of 12 and 18 m s^{-1} , respectively. Moreover, increasing VGRs from 43 to 64 levels (i.e., CTL64) leads to the development of more spiral rainbands that tend to suppress the eyewall convection, thus weaker storms (and weaker outflows) than OPN43. More rainbands with a weaker-than-OPN43 storm also occur in HLW64, HUP64, and UNM64 (Figs. 11d–f). However, the HLW64 storm is stronger than the HUP64 storm. Of relevance is that relatively stronger upward motions in the spiral rainbands occur near the altitudes of 6 km in HLW64, 6–8 km in HUP64, and 8–10 km*

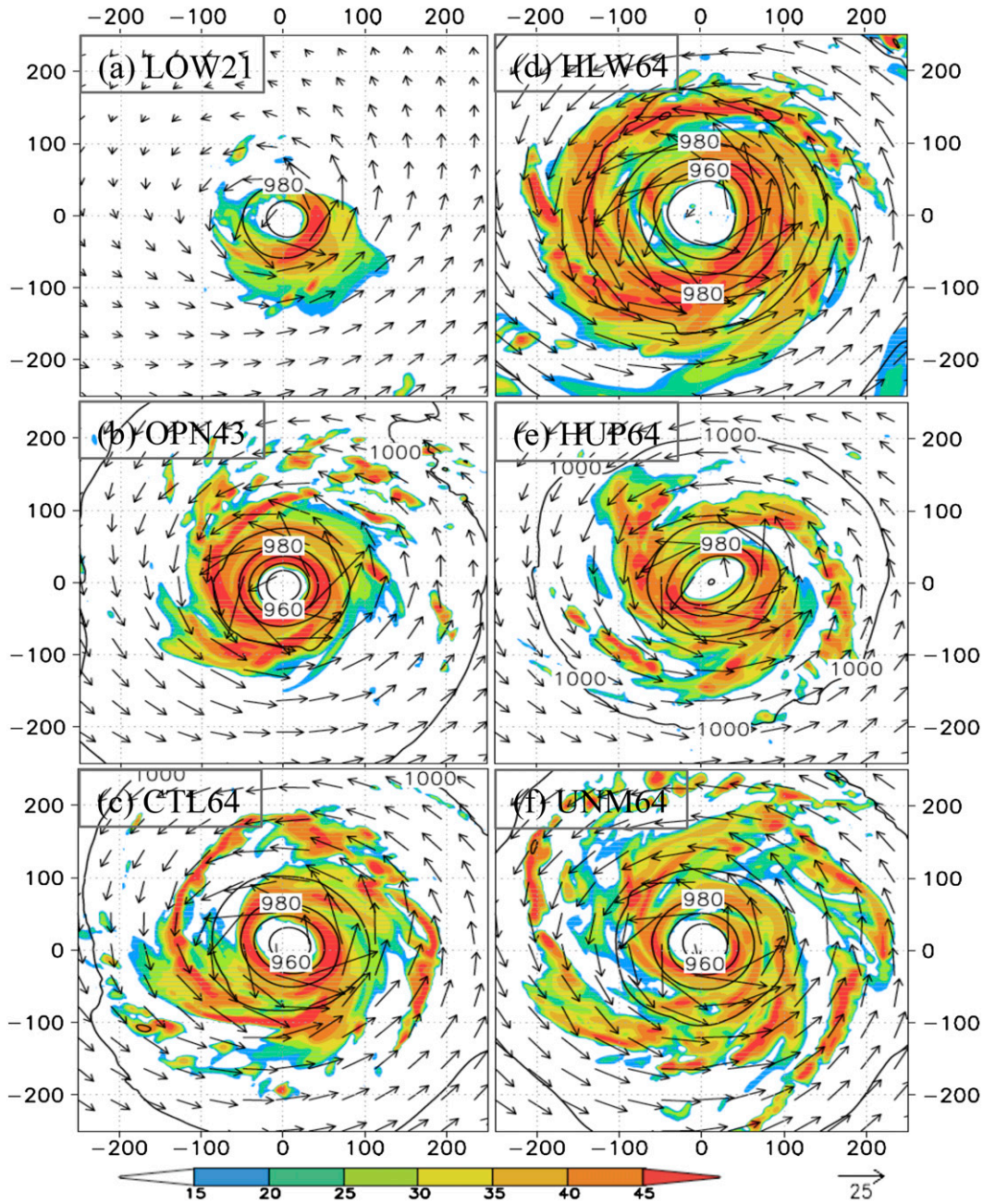


FIG. 10. Horizontal distribution of the simulated radar reflectivity (shadings), sea level pressure (contoured at intervals of 10 hPa), and surface wind vectors over a 500 km × 500 km subdomain of D3 from the 114-h simulations of (a) LOW21, (b) OPN43, (c) CTL64, (d) HLW64, (e) HUP64, and (f) UNM64 under the influence of no mean flow and no VWS (i.e., V0S0).

in UNM64, which are to some extent consistent with their increased VGRs at higher levels.

The above results may be understood as follows. Just like the impact of increased horizontal resolution (Δx) in nested-grid domains on the generation of larger mass convergence, increased VGRs (Δz) in any tropospheric layers would facilitate the generation of larger vertical

mass (ρ) convergence and moisture (q) flux convergence (i.e., $\partial \rho w / \partial z$ and $\partial w q / \partial z$) and gridbox saturation in those layers. This is because *the vertical flux convergence in hurricanes are driven more by diabatic heating than the larger-scale horizontal convergence*. Because of higher moisture content in the lower troposphere, increasing the lower-level VGRs tends to cause more latent heat

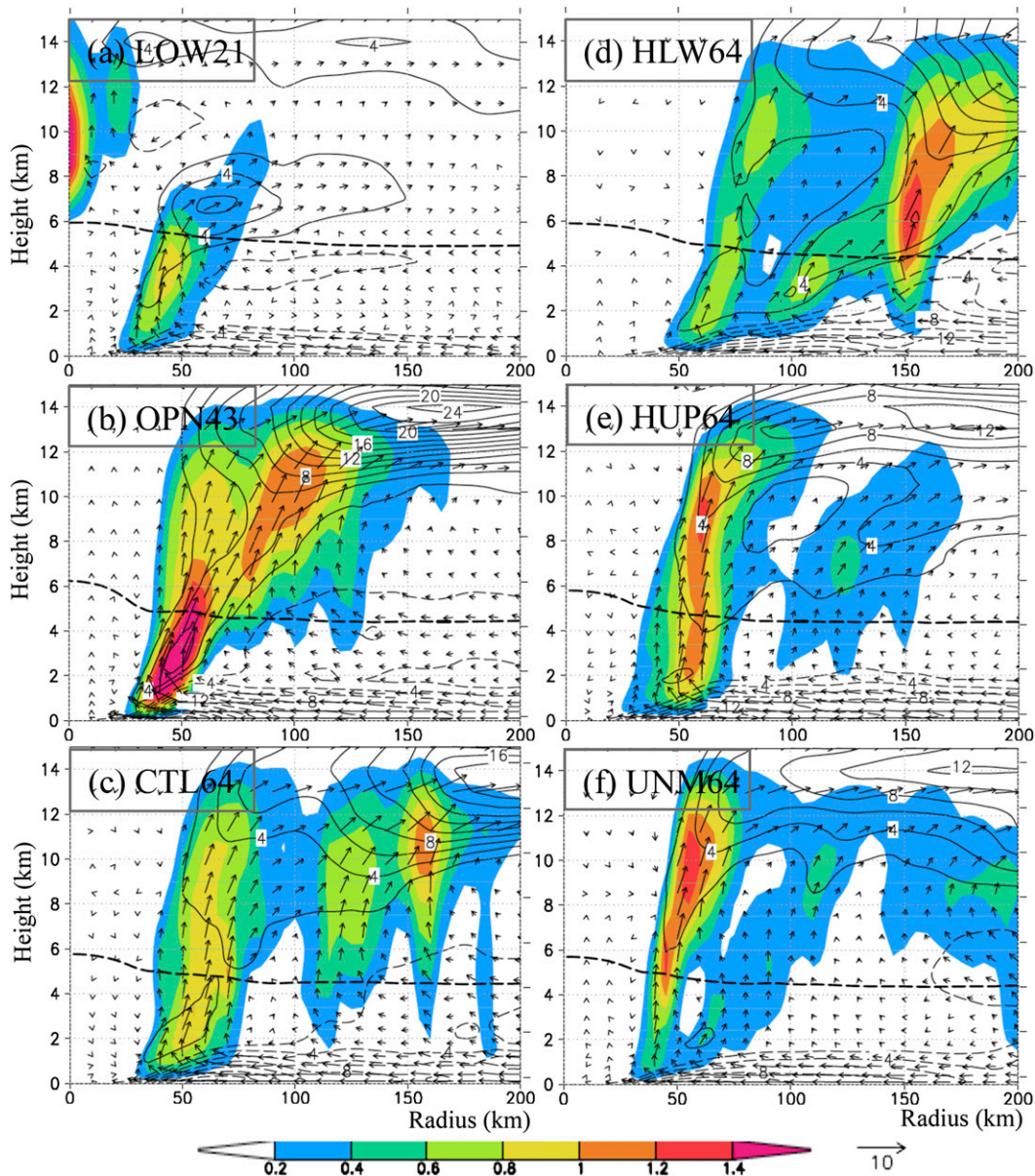


FIG. 11. As in Fig. 10, but for the radius–height cross sections of the azimuthally averaged vertical motion (shadings, m s^{-1}), radial winds contoured at intervals of 2 m s^{-1} , superimposed with in-plane flow vectors. Thick dashed lines denote the 0°C isotherm.

release than that with the increased upper-level VGRs. In addition to less latent heating in upper high-VGR layers, the subsequent horizontal convergence of the mid- and higher-level drier and colder air, as often indicated by an inflow layer above and below the upper outflow layer [see Chen and Zhang (2013)], is unfavorable for hurricane intensification. Note that the spiral rainbands in HUP64 and UNM64 are weaker in updraft intensity than those in CTL64 and HLW64. They are also attributable to the horizontal convergence and upward transport of relatively drier and colder air at the

mid- to upper levels in HUP64 and UNM64, in contrast to more moist air in the PBL in HLW64.

Similar insight could be gained from the soundings (Fig. 12) and the vertical distribution of associated dewpoint temperature depressions ($T - T_d$, Fig. 13) taken in the eyewall. Although all the simulations exhibit a lifting condensation level near $\sigma = 0.9$ with a near-saturated layer up to $\sigma = 0.75$, except for LOW21, the degree and layer thickness of saturation or $T - T_d$ appear to depend on VGRs used in different portions of the model atmosphere. Specifically, LOW21 produces $T - T_d = 0.5^\circ\text{C}$ in

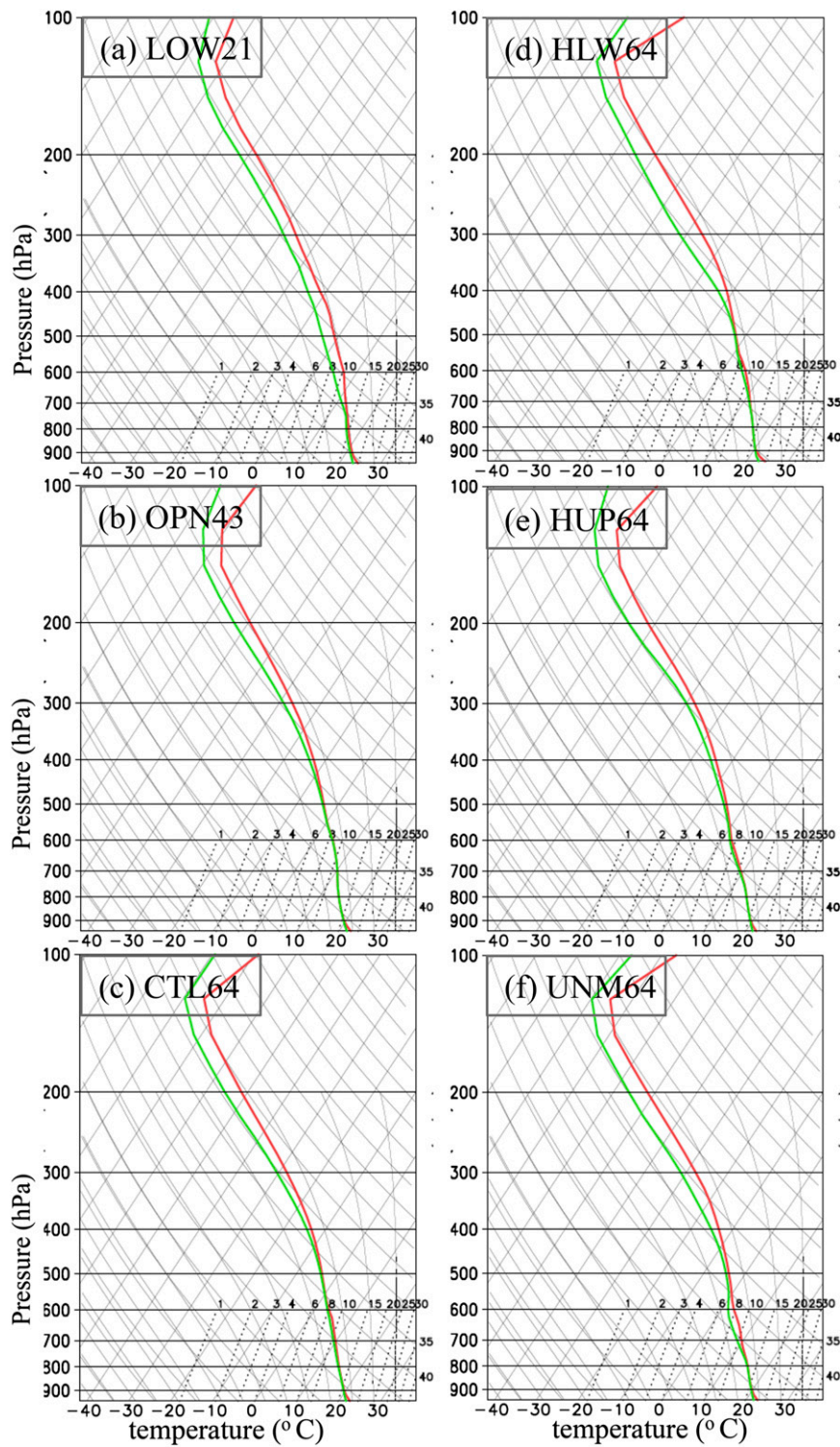


FIG. 12. As in Fig. 10, but for skew T -log p diagrams taken at the radius of the azimuthally averaged peak vertical motion in the eyewall.

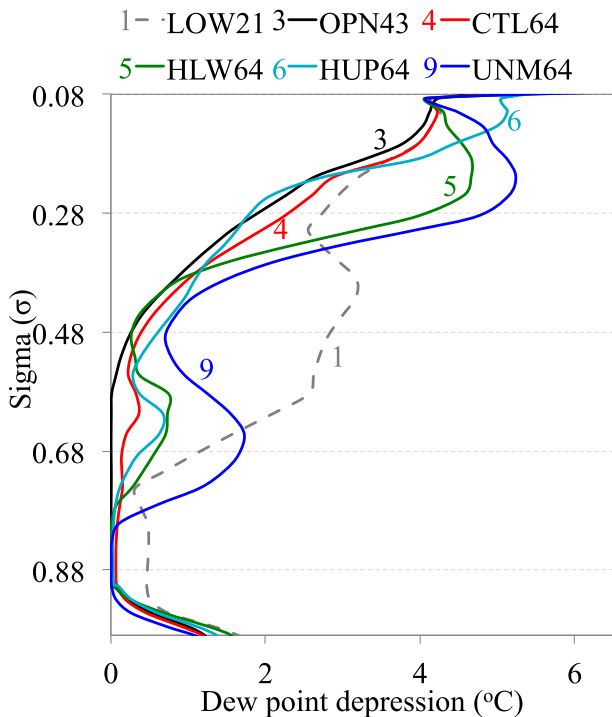


FIG. 13. Vertical distributions of dewpoint depressions as a function of σ ranging between 0.99 and 0.08, which are associated with the soundings given in Fig. 12. The same colors as those shown in Fig. 2 are used to represent the following six simulations: 1-LOW21, 3-OPN43, 4-CTL64, 5-HLW64, 6-HUP64, and 9-UNM64 obtained under the influence of no mean flow and no VWS (i.e., V0S0).

the $\sigma = 0.9$ – 0.75 layer in the eyewall, above which the model layer is conditionally stable with larger $T - T_d$ values. This is consistent with the shallow secondary circulations simulated (cf. Figs. 11a and 12a). By comparison, increasing VGR from 21 to 43 levels generates $T - T_d = 0.5^\circ\text{C}$ in the $\sigma = 0.75$ – 0.45 layer (Figs. 12b and 13), although increasing it further to 64 levels does not produce as deep a layer as in OPN43 (cf. Figs. 12b,c). Moreover, the two soundings even appear to be slightly absolutely unstable due to intense latent heat release at the updraft core. Of more relevance is that HUP64 shows markedly less $T - T_d$ in the $\sigma = 0.38$ – 0.18 layer than HLW64 (cf. Figs. 12e,d and 13); similarly for their corresponding updraft intensities (Figs. 11d–f).

Since larger intensity variability occurs when stronger VWS is imposed, Fig. 14 shows the inner-core rainfall and flow fields under V5S5. Several marked differences from those under V0S0 could be seen (cf. Figs. 14 and 10). They include the following: (i) more rainfall on the southern (i.e., downshear left) side of the hurricane vortices, as expected; (ii) much reduced rainfall coverage in all cases, especially with HLW64 and CTL64

(cf. Figs. 10c,d and 14b,c); and (iii) dissipating low-level circulations and less organized rainfall patterns, especially associated with HUP64, UNM64, and UNF64, in which little eyewall convection structures are present (Figs. 14d,f). All these results are consistent with the intensity differences shown in Fig. 8. In particular, point (iii) indicates again that the HWRF Model with increased upper- (lower-) level VGRs tends to produce weaker (stronger) storms with less (more) organized rainfall structures regardless of the presence of VWS.

In analyzing the inner-core structural differences under varying VWSs, we note the development of localized updrafts in the eyewall during the first 48-h integrations with VMAX20. These localized updrafts appear to produce varying effects on the spinup of hurricane vortices in HUP64, UNM64, and UNF64 (Figs. 6–8), as mentioned before. For this purpose, Fig. 15 compares the cloud hydrometeors and flow fields under V5S2.5 at $t = 7$ and 7.5 h, at which time some differences between HUP64 and OPN43 begin to emerge. The two runs are used herein because they only differ in VGR in the upper-half portion of the model atmosphere. We see vertically tilted vortex structures after the initial 7-h adjustment period, with the concentrated cloud ice content on the downshear side of the eyewall (Figs. 15a,d), where the shear-induced updraft peaks (Zhang and Kieu 2006). South–north vertical cross sections through the updraft cores show similar cloud water contents below the melting level between the two runs, but a larger volume of cloud ice and snow as well as stronger updrafts above in HUP64 than those in OPN43. This reveals clearly the significant role of increased VGR, starting from $\sigma = 0.5$, in intensifying gridbox saturation and updrafts. Such localized updrafts intensify rapidly in most cases under the influence of VWS, but more so in HUP64, UNM64, and UNF64, before more rainfall takes place on the downshear-left side of the eyewall. However, the localized updrafts (and their induced cyclonic vorticity, not shown) are more elevated (cf. Figs. 15b,e and 15c,f), and they interact negatively with the parent vortex, especially under V5S5, accounting for the weakening but generation of larger cyclonic circulations (Figs. 14d–f). In contrast, the localized updrafts (and vorticity) in the other simulations are more rooted in the PBL and tend to be organized by more intense vortex circulations in the lower troposphere, as opposed to much weaker cyclonic circulations (i.e., weaker shear deformation) aloft (e.g., in HUP64). Nevertheless, the localized features under V5S2.5 could be absorbed by the parent vortex after the 84-h integrations (Fig. 7), leading to the subsequent pronounced intensification of the HUP64 storm, as previously mentioned.

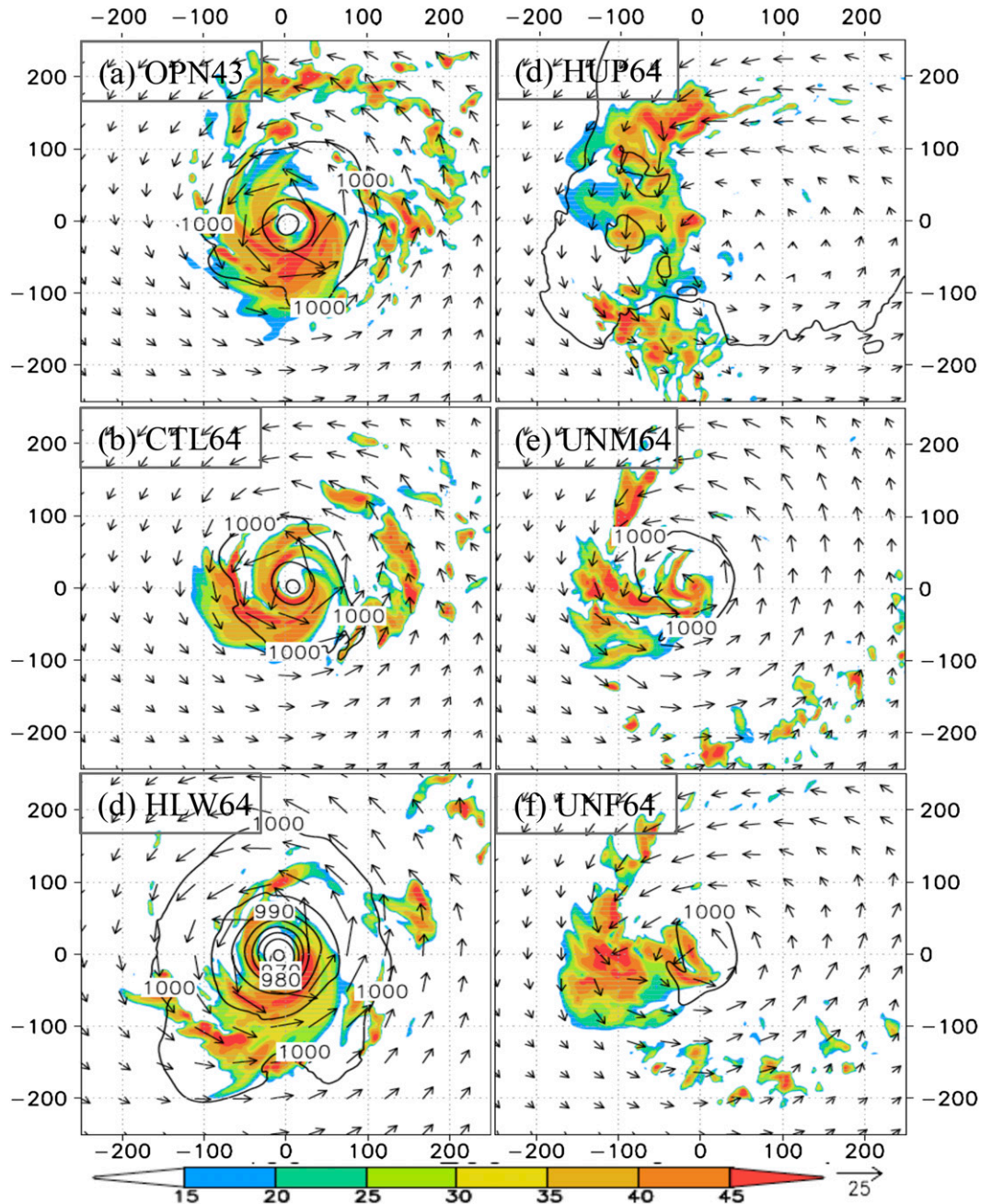


FIG. 14. As in Fig. 10, but for (a) OPN43, (b) CTL64, (c) HLW64, (d) HUP64, (e) UNM64, and (f) UNF64 under the influence of a 5 m s^{-1} easterly flow with a 5 m s^{-1} easterly VWS (i.e., V5S5).

6. Summary and conclusions

In this study, more than 63 five-day numerical simulations of two different idealized hurricane vortices under the influence of six different background flows are performed, using the HWRF Model with the finest 3-km grid length to examine the sensitivity of hurricane intensity to nine different distributions of VGR. Results

show that in the absence of background flow increasing VGR from 21 to 43 levels tends to produce ($10\text{--}15 \text{ m s}^{-1}$) stronger hurricanes in terms of P_{MIN} , V_{MAX} , and the upper outflow strength, but increasing it further to 64 levels produces ($5\text{--}10 \text{ m s}^{-1}$) weaker hurricanes. In addition, more pronounced intensity fluctuations occur in the simulations with lower VGRs (e.g., LOW21, LOW32, and OPN43). Of importance is that increasing the lower-level

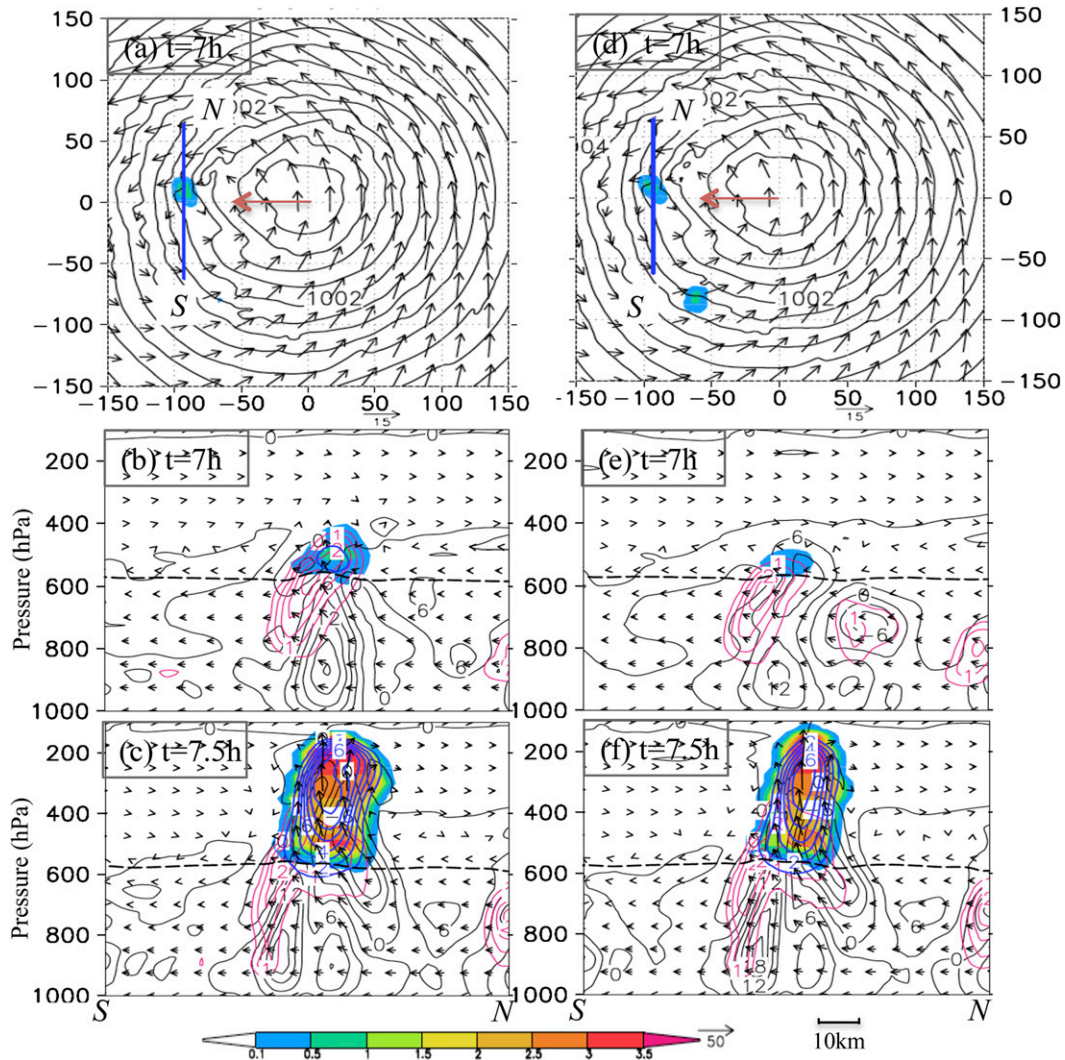


FIG. 15. Comparison of the cloud hydrometeors and flow fields under the influence of a 5 m s^{-1} easterly flow with a 2.5 m s^{-1} easterly VWS (i.e., V5S2.5) between (left) HUP64 and (right) OPN43, which are taken from a $400 \text{ km} \times 400 \text{ km}$ subdomain of D3. (a),(d) Horizontal distribution of the sea level pressure contoured at intervals of 1 hPa , cloud ice (shaded, $10^{-2} \text{ g kg}^{-1}$), and horizontal flow vectors at 500 hPa from the 7-h simulations. An orange arrow at the domain center denotes the VWS vector. (b),(e) Vertical cross sections of cloud ice (shaded, $10^{-2} \text{ g kg}^{-1}$), snow in black contours at intervals of 1 g kg^{-1} , and cloud water in purple contours at intervals of 1 g kg^{-1} , superimposed with in-plane flow vectors, along line S–N in (a) and (d) from the 7-h simulations. (c),(f) As in (b),(e), respectively, but from the 7.5-h simulations. The thick dashed lines in the vertical cross sections denote the 0°C isotherm.

VGR tends to produce a stronger storm (e.g., HLW64 and OMG64), whereas increasing the upper-level VGRs produces a weaker storm (i.e., HUP64). Similar characteristics also appear when background flows with or without VWS are imposed. Besides, adding a mean flow tends to increase intensity fluctuations and variability, whereas adding VWS delays hurricane intensification and subsequently causes more rapid growth in intensity variability. The largest intensity variability of 47 hPa and 48 m s^{-1} occurs in the presence of strong VWS (i.e., under V0S5), although it will likely continue to increase if the

sensitivity simulations were extended (e.g., under V0S5 and V5S5). Of further importance is that given the number of 64 vertical levels, hurricane intensity with the control- and omega-shaped VGRs (or higher VGRs in the lower levels) is the least sensitive to varying background flows, whereas the greatest sensitivity appears in the simulations with relatively uniform VGRs (i.e., UNM64 and UNF64) or higher VGRs in the upper levels (HUP64). We also find that the above VGR sensitivity depends on the initial vortex intensity, with less variability for a stronger hurricane vortex.

It is found that the above-mentioned intensity variations are closely associated with the inner-core rainfall structural changes. An analysis of the model simulated fields at an early hour reveals that stronger updrafts with more cloud particles or more near-saturated conditions occur in or near higher-VGR layers, confirming that gridbox saturation occurs more readily in or near the layers with higher VGRs. In this regard, we claim that increasing VGRs in cloud-resolving models could produce some impacts on hurricane development that are similar to increased horizontal resolution. This analysis explains why increasing VGRs from 43 levels in any portion of the troposphere tends to produce more rainbands and weaker storms. Because of higher moisture content in the lower troposphere, increasing the lower-level VGRs would enhance latent heat release and moisture convergence, and produce more convection and stronger storms than those with the increased upper-level VGRs. In contrast, colder and drier intrusion may occur near the upper-level higher-VGR layers. Some VGR configurations (e.g., LOW21, HUP64, UNM64, and UNF64) tend to produce little intensity changes under the influence of VWS, with quite different inner-core structures compared to the other VGRs runs. Localized circulations, generated by latent heating in the upper portion of the troposphere, are found in HUP64, due to the presence of less shear deformation associated with weaker rotation aloft.

The results presented above appear to provide some important hints for designing appropriate VGRs to predict reasonably hurricane intensity and inner-core structures under different environmental flows. First, certain minimum VGRs should be configured to produce reliable intensity forecasts with more detailed inner-core structures. Second, the near-parabolic or Ω -shaped vertical distribution of VGRs, with relatively higher (lower) VGRs in the lower (middle) levels, appear to be more preferable than higher VGRs in the upper levels. Third, if computing power is allowed, higher VGRs throughout the troposphere that are reasonably consistent with horizontal resolution (Lindzen and Fox-Rabinovitz 1989) should be utilized in order to produce smoother storm evolution with less fluctuations in intensity forecasts.

It should be mentioned that despite the many sensitivity simulations, some results may be limited to the idealized hurricane vortex and simple environmental conditions as well as to the HWRF's current configurations. Evidently, observed storm intensity and inner-core structures could provide useful validations to determine which VGR configurations perform better than the others. In a forthcoming study, we will examine the sensitivity of the HWRF-predicted hurricanes in an operational setting to the different VGRs used herein.

Acknowledgments. This work was supported by NOAA's Hurricane Forecast Improvement Project (HFIP) through Grants NA12NWS4680008 and NA12NWS4680007, NASA Grant NNX12AJ78G, and ONR Grant N000141410143. All the model integrations were conducted on NOAA's Jet computing system.

REFERENCES

- Anthes, R. A., and D. Keyser, 1979: Tests of a fine-mesh model over Europe and United States. *Mon. Wea. Rev.*, **107**, 963–984, doi:10.1175/1520-0493(1979)107<0963:TOAFMM>2.0.CO;2.
- Arakawa, A., and V. Lamb, 1977: Computational design of the basic dynamical process of the UCLA general circulation model. *Methods Comput. Phys.*, **17**, 173–265.
- Bao, J.-W., S. G. Gopalakrishnan, S. A. Michelson, F. D. Marks Jr., and M. T. Montgomery, 2012: Impact of physics representations in the HWRF on simulated hurricane structure and pressure–wind relationships. *Mon. Wea. Rev.*, **140**, 3278–3299, doi:10.1175/MWR-D-11-00332.1.
- Black, M. L., J. F. Gamache, F. D. Marks Jr., C. E. Samsury, and H. E. Willoughby, 2002: Eastern Pacific Hurricanes Jimena of 1991 and Olivia of 1994: The effect of vertical shear on structure and intensity. *Mon. Wea. Rev.*, **130**, 2291–2312, doi:10.1175/1520-0493(2002)130<2291:EPHJOA>2.0.CO;2.
- Chen, H., and D.-L. Zhang, 2013: On the rapid intensification of Hurricane Wilma (2005). Part II: Convective bursts and the upper-level warm core. *J. Atmos. Sci.*, **70**, 146–172, doi:10.1175/JAS-D-12-062.1.
- , —, J. Carton, and R. Atlas, 2011: On the rapid intensification of Hurricane Wilma (2005). Part I: Model prediction and structural changes. *Wea. Forecasting*, **26**, 885–901, doi:10.1175/WAF-D-11-00001.1.
- Davis, C., W. Wang, J. Dudhia, and R. Torn, 2010: Does increased horizontal resolution improve hurricane wind forecasts? *Wea. Forecasting*, **25**, 1826–1841, doi:10.1175/2010WAF2222423.1.
- Eckermann, S., 2009: Hybrid σ - p coordinate choices for a global model. *Mon. Wea. Rev.*, **137**, 224–245, doi:10.1175/2008MWR2537.1.
- Ferrier, B. S., 1994: A double-moment multiple-phase four-class bulk ice scheme. Part I: Description. *J. Atmos. Sci.*, **51**, 249–280, doi:10.1175/1520-0469(1994)051<0249:ADMMPF>2.0.CO;2.
- , 2005: An efficient mixed-phase cloud and precipitation scheme for use in operational NWP models. *Spring Meeting 2005*, San Francisco, CA, Amer. Geophys. Union, Abstract A42A-02.
- Fierro, A. O., R. F. Rogers, F. D. Marks, and D. S. Nolan, 2009: The impact of horizontal grid spacing on the microphysical and kinematic structures of strong tropical cyclones simulated with the WRF-ARW model. *Mon. Wea. Rev.*, **137**, 3717–3743, doi:10.1175/2009MWR2946.1.
- Frank, W. M., and E. A. Ritchie, 1999: Effects of environmental flow upon tropical cyclone structure. *Mon. Wea. Rev.*, **127**, 2044–2061, doi:10.1175/1520-0493(1999)127<2044:EOEFUT>2.0.CO;2.
- , and —, 2001: Effects of vertical wind shear on hurricane intensity and structure. *Mon. Wea. Rev.*, **129**, 2249–2269, doi:10.1175/1520-0493(2001)129<2249:EOVWSO>2.0.CO;2.
- Gopalakrishnan, S. G., F. D. Marks Jr., X. Zhang, J.-W. Bao, K.-S. Yeh, and R. Atlas, 2011: The experimental HWRF system: A study on the influence of horizontal resolution on the structure and intensity changes in tropical cyclones using an idealized

- framework. *Mon. Wea. Rev.*, **139**, 1762–1784, doi:10.1175/2010MWR3535.1.
- , —, J. A. Zhang, X. Zhang, J.-W. Bao, and V. Tallapragada, 2013: A study of the impacts of vertical diffusion on the structure and intensity of the tropical cyclones using the high-resolution HWRf system. *J. Atmos. Sci.*, **70**, 524–541, doi:10.1175/JAS-D-11-0340.1.
- Gray, W. M., E. Ruprecht, and R. Phelps, 1975: Relative humidity in tropical weather systems. *Mon. Wea. Rev.*, **103**, 685–690, doi:10.1175/1520-0493(1975)103<0685:RHITWS>2.0.CO;2.
- Han, J., and H.-L. Pan, 2006: Sensitivity of hurricane intensity forecasts to convective momentum transport parameterization. *Mon. Wea. Rev.*, **134**, 664–674, doi:10.1175/MWR3090.1.
- Hong, S.-Y., and H.-L. Pan, 1996: Nonlocal boundary layer vertical diffusion in a medium-range forecast model. *Mon. Wea. Rev.*, **124**, 2322–2339, doi:10.1175/1520-0493(1996)124<2322:NBLVDI>2.0.CO;2.
- Janjić, Z. I., 2003: A nonhydrostatic model based on a new approach. *Meteor. Atmos. Phys.*, **82**, 271–285, doi:10.1007/s00703-001-0587-6.
- , J. P. Gerrity, and S. Nickovic, 2001: An alternative approach to nonhydrostatic modeling. *Mon. Wea. Rev.*, **129**, 1164–1178, doi:10.1175/1520-0493(2001)129<1164:AAATNM>2.0.CO;2.
- , R. Gall, and M. E. Pyle, 2010: Scientific documentation for the NMM solver. NCAR Tech. Note NCAR/TN-477+STR, doi:10.5065/D6MW2F3Z, 54 pp. [Available online at <http://openky.library.ucar.edu/collections/TECH-NOTE-000-000-000-845>.]
- Kimball, S. K., and F. C. Dougherty, 2006: The sensitivity of idealized hurricane structure and development to the distribution of vertical levels in MM5. *Mon. Wea. Rev.*, **134**, 1987–2008, doi:10.1175/MWR3171.1.
- Kwon, Y. C., S. Lord, B. Lapenta, V. Tallapragada, Q. Liu, and Z. Zhang, 2010: Sensitivity of air-sea exchange coefficients (Cd and Ch) on hurricane intensity. *29th Conf. on Hurricanes and Tropical Meteorology*, Tucson, AZ, Amer. Meteor. Soc., 13C.1. [Available online at https://ams.confex.com/ams/29Hurricanes/techprogram/paper_167760.htm.]
- Lacis, A. A., and J. E. Hansen, 1974: A parameterization for the absorption of solar radiation in the earth's atmosphere. *J. Atmos. Sci.*, **31**, 118–133, doi:10.1175/1520-0469(1974)031<0118:APFTAO>2.0.CO;2.
- Lindzen, R. S., and M. Fox-Rabinovitz, 1989: Consistent vertical and horizontal resolution. *Mon. Wea. Rev.*, **117**, 2575–2583, doi:10.1175/1520-0493(1989)117<2575:CVAHR>2.0.CO;2.
- Liu, Y., D.-L. Zhang, and M. K. Yau, 1997: A multiscale numerical study of Hurricane Andrew (1992). Part I: An explicit simulation. *Mon. Wea. Rev.*, **125**, 3073–3093, doi:10.1175/1520-0493(1997)125<3073:AMNSOH>2.0.CO;2.
- Peng, M. S., B. F. Jeng, and R. T. Williams, 1999: A numerical study on tropical cyclone intensification. Part I: Beta effect and mean flow effect. *J. Atmos. Sci.*, **56**, 1404–1423, doi:10.1175/1520-0469(1999)056<1404:ANSOTC>2.0.CO;2.
- Powell, M. D., 1990: Boundary layer structure and dynamics in outer hurricane rainbands. Part II: Downdraft modification and mixed layer recovery. *Mon. Wea. Rev.*, **118**, 918–938, doi:10.1175/1520-0493(1990)118<0918:BLSADI>2.0.CO;2.
- Schwarzkopf, M. D., and S. Fels, 1991: The simplified exchange method revisited: An accurate, rapid method for computation of infrared cooling rates and fluxes. *J. Geophys. Res.*, **96**, 9075–9096, doi:10.1029/89JD01598.
- Tallapragada, V., and Coauthors, 2013: Hurricane Weather Research and Forecasting (HWRf) Model: 2013 scientific documentation. Developmental Testbed Center, 99 pp. [Available from <http://www.dtcenter.org/HurrWRF/users/docs/>.]
- Tracton, M. S., 1973: The role of cumulus convection in the development of extratropical cyclones. *Mon. Wea. Rev.*, **101**, 573–592, doi:10.1175/1520-0493(1973)101<0573:TROCCI>2.3.CO;2.
- Wang, Y., and G. J. Holland, 1996: Tropical cyclone motion and evolution in vertical shear. *J. Atmos. Sci.*, **53**, 3313–3332, doi:10.1175/1520-0469(1996)053<3313:TCMAEI>2.0.CO;2.
- Yau, M. K., Y. Liu, D.-L. Zhang, and Y. Chen, 2004: A multiscale numerical study of Hurricane Andrew (1992). Part VI: Small-scale inner-core structures and wind streaks. *Mon. Wea. Rev.*, **132**, 1410–1433, doi:10.1175/1520-0493(2004)132<1410:AMNSOH>2.0.CO;2.
- Yeh, K.-S., X. Zhang, S. Gopalakrishnan, S. Aberson, R. Rogers, F. Marks, and R. Atlas, 2012: Performance of the experimental HWRf in the 2008 hurricane season. *Nat. Hazards*, **63**, 1439–1449, doi:10.1007/s11069-011-9787-7.
- Zhang, D.-L., and J. M. Fritsch, 1988: Numerical sensitivity experiments of varying model physics on the structure, evolution, and dynamics of two mesoscale convective systems. *J. Atmos. Sci.*, **45**, 261–293, doi:10.1175/1520-0469(1988)045<0261:NSEOVM>2.0.CO;2.
- , and X. Wang, 2003: Dependence of hurricane intensity and structures on vertical resolution and time-step size. *Adv. Atmos. Sci.*, **20**, 711–725, doi:10.1007/BF02915397.
- , and C. Q. Kieu, 2006: Potential vorticity diagnosis of a simulated hurricane. Part II: Quasi-balanced contributions to forced secondary circulations. *J. Atmos. Sci.*, **63**, 2898–2914, doi:10.1175/JAS3790.1.
- Zhang, F., and D. Tao, 2013: Impacts of vertical wind shear on the predictability of tropical cyclones. *J. Atmos. Sci.*, **70**, 975–983, doi:10.1175/JAS-D-12-0133.1.
- Zhang, X., K.-S. Yeh, T. S. Quirino, S. G. Gopalakrishnan, F. D. Marks, S. B. Goldenberg, and S. Aberson, 2011: HWRfX: Improving hurricane forecasts with high-resolution modeling. *Comput. Sci. Eng.*, **13**, 13–21, doi:10.1109/MCSE.2010.121.
- Zhu, T., D.-L. Zhang, and F. Weng, 2004: Numerical simulation of Hurricane Bonnie (1998). Part I: Eyewall evolution and intensity changes. *Mon. Wea. Rev.*, **132**, 225–241, doi:10.1175/1520-0493(2004)132<0225:NSOHBP>2.0.CO;2.